# RSC Advances

ROYAL SOCIETY
OF **CHEMISTRY**

www.rsc.org/advances
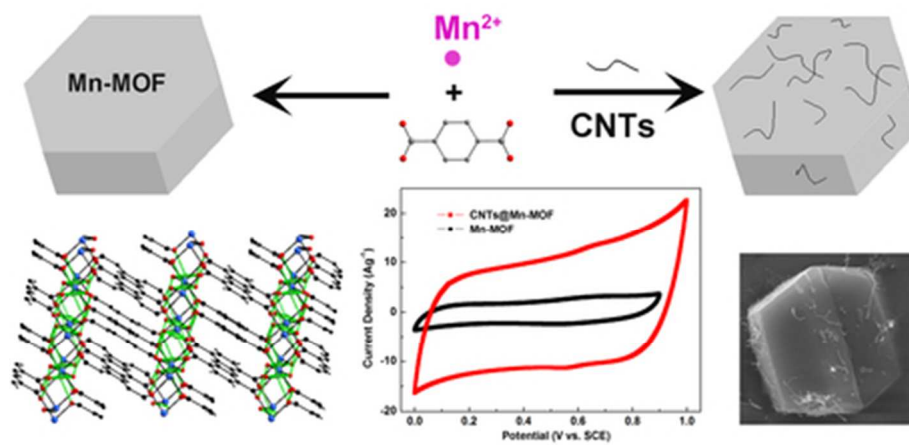
38x19mm (300 x 300 DPI)

# Journal Name

## ARTICLE

# Carbon nanotubes@metal-organic frameworks as Mn-based symmetrical supercapacitor electrodes for enhanced charge storage†

Yidong Zhang, Baoping Lin*, Ying Sun, Xueqin Zhang, Hong Yang, Junchuan Wang

A hybrid material of carbon nanotubes (CNTs) and Mn-based metal organic frameworks (Mn-MOF) was synthesized and used as the Mn-based supercapacitor electrode material. The incorporation of CNTs into Mn-MOF leaded to an inherent improvement in conductivity and an intrinsic increase in specific capacitance (from 43.2 F $g^{-1}$ for pure Mn-MOF to 203.1 F $g^{-1}$ for CNTs@Mn-MOF). Furthermore, the symmetrical supercapacitor based on the CNTs@Mn-MOF exhibited excellent power density and outstanding stability even after 3000 cycles with 88% retention of the initial capacitance. This research exploited a new direction for developing Mn-based supercapacitor materials and provided an effective method to improve capacitive performance of MOFs materials.

## Introduction

Recently, supercapacitor electrode materials, such as the oxides of Ru, Ni, Co, Cu, Fe, V and Mn, have attracted great research interests because of their excellent pseudocapacitance.[1] Among them, manganese oxides ($MnO_x$) are considered to be the most promising electrode materials due to their wide potential ranges, low-cost and environmentally friendly nature.[2,3] To date, Mn-based supercapacitor materials can be classified into two broad categories: pure $MnO_x$ with various crystal structures and hybrid composites of $MnO_x$.[4] In the former category, $MnO_x$ without any doping have been directly used as electrode materials, including $MnO$, $MnO_2$, $Mn_2O_3$, $Mn_3O_4$.[5-11] However, these single materials often produce low capacitances and weak cycle stabilities due to their poor electrical conductivities. Therefore, various hybrid composites of $MnO_x$ have been synthesized to overcome this shortage. The materials used to dope $MnO_x$ are mainly in three cases: carbon materials such as carbon black, acetylene black, CNTs and exfoliated graphite;[12-14] metal oxides including oxides of Ni, Ru, Cu, Fe, Co, Mo and Ag;[15,16] and conducting polymers *e.g.* polyaniline, poly(3-methylthiophene), poly(3,4-ethylenedioxythiophene) and polypyrrole.[17,18] Though such hybrid composites of $MnO_x$, to some extent, have showed better electrical conductivities than pure $MnO_x$ materials, they produced a number of new disadvantages at the same time, such as reduction of capacitance, increase of inherent contact resistances and structural instability. Therefore, it is essential to develop new Mn-based electrode materials to ameliorate these problems.

*School of Chemistry and Chemical Engineering, Southeast University, Nanjing 211189, China. E-mail: lbp@seu.edu.cn; Tel./fax: +86-25-52090616.*
† Electronic Supplementary Information (ESI) available: Further details for structural figures, GCD, and EIS. See DOI: 10.1039/x0xx00000x

Metal-organic frameworks (MOFs) have received huge attention as attractive materials with chemical and structural diversity in recent years. Compared with traditional materials, MOFs show significant advantages due to their high accessible surface areas, tuneable pore sizes, open metal sites and ordered crystalline structures.[19] They have been widely applied in many area such as catalysis,[20] gas separation,[21] drug storage and delivery,[22] imaging and sensing,[23] ptoelectronics[24] or energy storage.[25,26] However, the investigation of MOFs used as electrode materials for supercapacitors is quite lacking. In the original studies, MOFs were only employed as templates for the preparation of either nano–micro scale metal-oxide materials or microporous carbon materials.[27-30] Until recently, more and more MOFs based on various metals were directly used as electrode materials for supercapacitors. Thus, in the following paragraph we will make a short overview of the most relevant reports.

To the best of our knowledge, the first report demonstrating MOFs as supercapacitor materials has been made by D.Y. Lee *et al.*,[31] in which the Co-MOF material was deposited on an Indium doped Tin Oxide (ITO) substrate as a film to form the working electrode. This material showed a specific capacitance of 206.76 F $g^{-1}$ and a loss of only 1.5% in capacitance for 1000 electrochemical life cycle stability test. Another three Co-based MOFs were synthesized by the same authors to study the influence of MOFs microstructure on the electrochemical properties by controlling the length of organic linkers.[32] The best of them exhibited supercapacitive properties with 179.2 F $g^{-1}$, 31.4 Wh $kg^{-1}$ and 5.64 kW $kg^{-1}$ of specific capacitance, energy density and power density, respectively. Afterwards, two porous MOFs based on Zn and Cd which were deposited on glassy carbon electrodes were reported by J. Lin provided capacitance values of 23 and 22 F $g^{-1}$, respectively.[33] Further, M. Du reported a mesoporous In-based MOF material with 1-D

hexagonal channels, which provided a capacitance of 81 F g$^{-1}$ (1 A g$^{-1}$) and maintain about 100% of its maximum value after cycling 6000 times.[34] Almost immediately, a series of Fe-based MOFs were synthesized with a best capacitance of 57.5 Fg$^{-1}$ in 0.1M K$_2$SO$_4$ solution.[35] Obviously, the above MOFs materials have had limited success in supercapacitor. Nevertheless, the Ni-based MOF[36] with layered structure and Zn-doped Ni-MOF[37] with a flower-like microsphere were successfully synthesized by M. Wei and co-workers, both of which displayed high specific capacitance, good rate capability and good cycling stability. They found that the outstanding electrochemical properties were attributed to the intrinsic characteristics of the MOFs including layered structure, enlarged interlayer distance and porous feature. Between the two reports, Kang et al. carried out a study of 23 different graphene-doped nMOFs,[38] in which a series of Zr-, Co-, Ni-, Zn- and Cu-based MOFs have been researched in detail. Particularly, graphene was doped into nMOFs as a physical mixture to increase the conductivity of the materials. And the electrochemical tests demonstrated that several of the graphene-doped nMOFs showed good performance, the Zr-MOF material could even reach a high specific capacitance of 726 F g$^{-1}$ at a current density of 0.88 mA cm$^{-3}$. However, the graphene was dispread in organic solvent for several times before it was coated on electrode. In the latest report, a composite material of Cu-based MOF and reduced graphene oxide (rGO) exhibited a specific capacitance of 385 F g$^{-1}$ at 1A g$^{-1}$, which was spray-coated on carbon fiber paper to fabricate a supercapacitor.[39] Though the method was relatively effective to improve the electrical properties of MOFs, it was cumbersome and complicated. Thus, it is quite necessary to find a new method to modify MOFs, which is not only effective but also simple. In addition, another important phenomenon has caught our attention. Basically, all commonly used metals have been studied as MOFs materials for supercapacitors except for manganese. Meanwhile, the Mn-based materials, typically possessing wider potential ranges in comparison with other metal based materials, have played an important role in supercapacitor materials for a long time. Therefore, it is necessary to introduce Mn-based MOFs as supercapacitor electrode materials and further, find a simple and effective method to modify them for excellent capacitance, great structural flexibility and good cycle stability. One effective modification approache is to incorporate carbon nanotubes(CNTs) into MOFs, which can obviously improve the properties of MOF materials.[40,41] The use of CNTs as composite fillers has been investigated in various MOFs, such as MOF-5[42] and HKUST-1,[43,44] in which the CNTs with carboxylic groups provide homogeneous nucleation sites to support a continuous metal framework growth. Herein, modifying MOFs with CNTs can eliminate most of the limitations of traditional Mn-based electrode materials. Motivated by these results, we fabricated a hybrid MOF material by incorporating CNTs into a facile Mn-MOF with a simple hydrothermal method for high-performance supercapacitive energy storage.

In the present work, a composite of Mn(C$_8$H$_4$O$_4$)(H$_2$O)$_2$ (where H$_2$C$_8$H$_4$O$_4$ = *p*-benzenedicarboxylic acid)[45] incorporated with CNTs was successfully synthesized and used as a new type of Mn-based supercapacitor electrode material. The specific capacitance values of this material was 7.1- and 15-fold higher than those of the pure Mn-MOF at 1 and 20 A g$^{-1}$, respectively. A symmetric supercapacitor of the CNTs@Mn-MOF was fabricated, and it displayed an maximum energy density of 6.9 Wh kg$^{-1}$ and a maximum power density of 2240 W kg$^{-1}$. All the materials and their electrochemical properties were investigated in detail.

## Experimental details

### Materials preparation

**Preparation of Carboxyl CNTs.** Carbon nonotubes were soaked in a mixed acid (including equal parts of concentrated nitric acid and concentrated sulfuric acid) for 8 h at 80 °C in oil bath with stirring, recovered by filtration, washed with deionized water, and dried at 50 °C. The short acidification time results microscale carboxyl CNTs.

**Preparation of Mn-MOF.** Mn-MOF was synthesized according to a previous report after a minor modification.[45] In a typical procedure, a solution of 1.0080 g of (NH$_4$)$_2$C$_8$H$_4$O$_4$ in a mixture of 20 ml of ethanol and 40 ml deionized water was filtered to remove a trace of insoluble material. A solution of 1.4578 g of Mn(C$_2$H$_4$O$_2$)$_2$(H$_2$O)$_4$ in 40 ml deionized water was added slowly with stirring. The solution was stirred at room temperature for 30 min and was transformed into a Teflon-lined stainless steel autoclave with a capacity of 35 ml, and was kept at 85 °C for 24 h. After cooling to room temperature, the resulting precipitate was washed with deionized water and alcohol several times. Finally, the final products were dried at 70 °C for 12 h in vacuums and the Mn-based MOF material were obtained.

**Preparation of CNTs@Mn-MOF.** CNTs@Mn-MOF was synthesized according to a previous report after a minor modification.[43] CNTs/ethanol (20 mL) was mixed with 40 mL deionized water containing predissolved Mn(C$_2$H$_3$O$_2$)$_2$(H$_2$O)$_4$ (1.4578 g). The resulting mixture was sonicated for 30 min and was then kept stirring at room temperature for 48 h. After that, a solution of 1.0080 g of (NH$_4$)$_2$C$_8$H$_4$O$_4$ in 40 ml deionized water was added slowly with stirring. Further procedures were similar to synthesis of Mn-MOF.

### Material characterizations

X-ray diffraction (XRD) patterns were recorded on Bruker D8 Advance X-ray diffractometer using Cu K$\alpha$ radiation (40 kV, 200 mA). Scanning electron microscopy (SEM) and transmission electron microscopy (TEM) were carried out on a FEI Sirion 200 at an accelerating voltage of 5.0 kV and a Tecnai G2 T20 (FEI) operated at 200 kV, respectively. Fourier Transform Infrared (FT-IR) transmission spectra were recorded on a BRUKER-EQUINOX-55 IR spectrophotometer. The thermogravimetric analysis (TGA) was operated on TA Instruments SDT-Q600 with the heating rate of 20 °C min$^{-1}$ under ambient conditions. X-ray photoelectron spectroscopy

(XPS) measurements were performed with a Thermo Scientific K-Alpha using monochromatic Al K$\alpha$ radiation.

**Electrochemical measurements**

**Single electrodes.** Cyclic voltammetry (CV), galvanostatic charge–discharge (GCD) measurements and electrochemical impedance spectroscopy (EIS) were obtained from an electrochemical working station (CHI 660e, Chenghua, Shanghai) using a standard three-electrode cell at ambient temperature. The working electrode was prepared by mixing 80 wt% active material, 10 wt% acetylene black and 10 wt% of polytetrafluoroethylene binder, and then coated on carbon fibre paper. The mass loading of the sample is about 1.2 mg cm$^{-2}$. After drying, the electrodes were impregnated with 1 M Na$_2$SO$_4$ electrolyte under vacuum. A platinum wire and a saturated calomel electrode (SCE) were used as the counter and reference electrodes, respectively. The EIS data were collected with an AC voltage of 10 mV amplitude in the frequency range from 1 MHz to 0.1 Hz. The gravimetric specific capacitance Cg was calculated based on the equation:

$$Cg = I \times \Delta t /(m \times \Delta V)$$

where $I$, $\Delta t$, $\Delta V$ and m denote the applied current, discharge time, voltage change and the mass of the active material, respectively.

**Symmetrical supercapacitors.** The symmetrical supercapacitors were constructed via a two electrode configuration in 1 M Na$_2$SO$_4$ aqueous electrolyte with one piece of polypropylene membrane as a separator. The CNTs@Mn-MOF composites were used as both anode and cathode electrodes. The electrodes were prepared by mixing 80 wt% active material, 10 wt% acetylene black and 10 wt% of polytetrafluoroethylene binder, and then coated on carbon fibre paper, respectively. The mass loading of the sample is about 1 mg cm$^{-2}$. The specific capacitance of the symmetrical supercapacitor ($C_{cell}$) was calculated by the equation:

$$1 / C_{cell} = (1 / C_+ + 1 / C_-) = I \times (\Delta t / \Delta V) \times (1 / m_+ + 1 / m_-)$$

where $C_+$ and $C_-$ are the specific capacitances of the positive and negative electrodes as well as $m_+$ and $m_-$ are the mass of active materials in positive and negative electrodes, respectively. The average specific energy ($E$) and specific power ($P$) are calculated from $E = 1 / 2\, C_{cell} (\Delta V)^2$ and $P = E / \Delta t$, respectively.

## Results and discussion

The CNTs@Mn-MOF composites and Mn-MOF were synthesized by a facile hydrothermal method. The Mn-MOF structure (Fig. S1†) consists of alternating layers which were perpendicular to direction $a$. And these layers were connected by hydrogen bonds between Mn-coordinated water molecules. Each layer was built up from one-dimensional (1D) chains of terephthalate anions and octahedrally coordinated metal cations extended parallel to the $a$-axis. Fig. 1 shows the detail hydrogen-bonding network in Mn-MOF. The delineating of the structure suggests two potential hydrogen bonds between each water-molecule H atom and a carboxylate O atom. These abounding hydrogen-bonds, which ensure cohesion of the
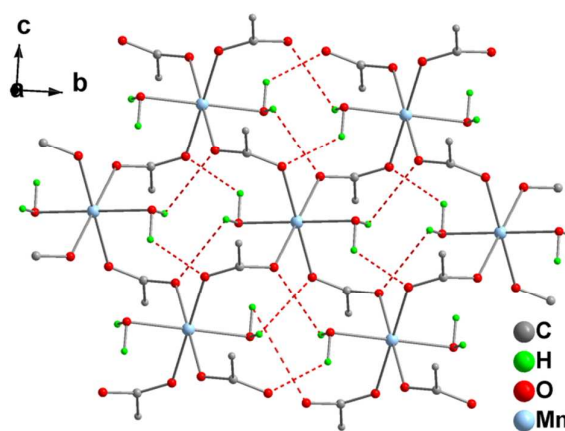


**Fig. 1** The hydrogen-bonding network in Mn-MOF.

structure, connected the 1-D layers into 3-D networks. And notably, two reported Ni-MOF had been confirmed to achieve excellent electrochemical performance due to the same layers-hydrogen bonds structure.[36,37] The morphologies and structures of the CNTs@Mn-MOF composites were examined by SEM and TEM (Fig. 2). The CNTs@Mn-MOF morphology was characterized by well-defined hexagonal blocks 3-8 μm in each edge lenth (Fig. 2a). The regularly stick-like dents on the smooth crystal surface (Fig. 2b) indicated that CNTs were incorporated inside Mn-MOF, which was clearly displayed in TEM (Fig. 2c, 2d). The micron-scale blocks were grinded to fragments to obtain an observable sample before test. The CNTs embedded in the sheets, which act as composite fillers in the MOF crystal, can be seen clearly from the TEM image. As presumed in the previous report, the CNTs@Mn-MOF crystals were formed by heteronucleation and crystal growth on the carboxylic groups of the CNTs.[42]

To investigate the filling of CNTs in more details, the composites were examined by various methods. Fig. 3a exhibits
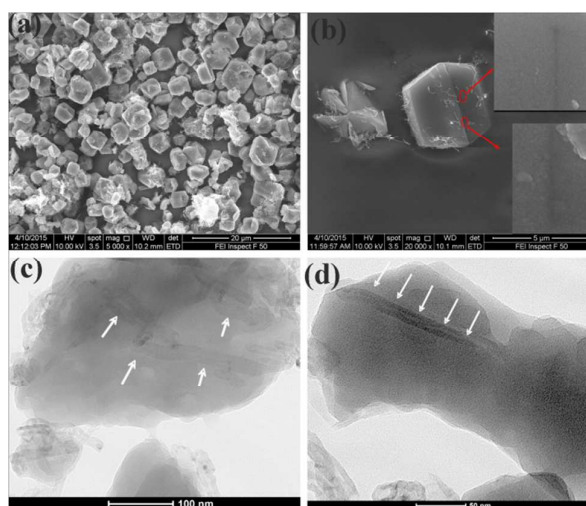


**Fig. 2** (a and b) SEM (the inset shows an enlarged view of the crystal surface), (c and d) TEM of CNTs@Mn-MOF in different views (white arrows indicate CNTs).
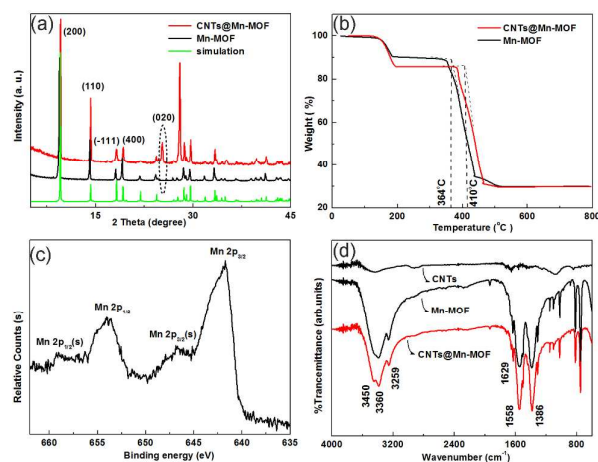
**Fig. 3** Characterization results of CNTs@Mn-MOF and Mn-MOF: (a) XRD patterns, (b) TG curves, (c) XPS, and (d) FTIR spectra.

the powder XRD patterns of Mn-MOF and CNTs@Mn-MOF. The diffraction pattern of the Mn-MOF was in good consistent with that simulated from the single-crystal data of $Mn(C_8H_4O_4)(H_2O)_2$(CCDC 195798).[45] In contrast, the powder XRD pattern of CNTs@Mn-MOF presented a new peak at $2\theta =$ 26-27°, which normally corresponded to the (0 0 2) plane of the CNTs component. All of the other diffraction peaks for CNTs@Mn-MOF showed that the sketch of the Mn-MOF crystal was well retained even after modification with the CNTs. TG curves, shown in Fig. 3b, indicated that incorporating CNTs enhanced thermal stability of Mn-MOF. An initial weight loss of 14.1% up to 190 °C was due to the loss of solvated water molecules in Mn-MOF, and it was less than that in CNTs@Mn-MOF because of the pore activation by CNTs. Furthermore, CNTs in Mn-MOF enhanced thermal stability, as demonstrated by a rise in decomposition temperature from 364 to 410 °C, which corresponded to the initial decomposition of Mn-MOF to yield manganese oxides. The behavior of TGA was consistent with the previous reports.[42,43] Fig. 3c shows the XPS analysis. The major peaks centred at around 641.8, 646.5, 653.7 and 658.0 eV, corresponding to Mn $2p_{3/2}$, Mn $2p_{3/2}$ satellites, Mn $2p_{1/2}$ and Mn $2p_{1/2}$ satellites, respectively, which were characteristic of $Mn^{2+}$ and in good agreement with previous literature reports.[46] The FTIR spectra of CNTs, Mn-MOF and CNTs@Mn-MOF were shown in Fig. 3d. As for Mn-MOF, the asymmetric stretching of the carboxylate group in the terephthalic acid linker appeared at around 1629 and 1558 cm$^{-1}$ and its symmetric stretching appeared around 1386 cm$^{-1}$. The stretching vibrations of water molecules at around 3450, 3360 and 3259 cm$^{-1}$ indicated that coordinated $H_2O$ molecules were present within the Mn-MOF material.[45,47] FTIR spectrum of Mn-MOF was found to be in agreement with the previous literature report.[36] Compared with the spectra of Mn-MOF and CNTs, the relevant CNTs peaks in CNTs@Mn-MOF, which normally around 1629 and 1386 cm$^{-1}$, were swamped by the high intensity Mn-MOF peaks. Therefore, the FTIR spectrum of CNTs@Mn-MOF was similar to that of Mn-MOF. The various characterization suggests that

we successfully incorporated CNTs into Mn-MOF, and a novel CNTs@Mn-MOF composite material was obtained.

To investigate the supercapacitive performance of CNTs@Mn-MOF as electrode material, we carried out electrochemical measurements by using an electrochemical workstation. Its capacitive behavior was first investigated by CV in Fig. 4. As well as the reported CV curves for MnO@C materials, the slight kink in the redox peak was also observed for the CNTs@Mn-MOF, which were thought to be caused by faradaic reactions of the electrode materials and carbon.[48,49] The proposed reaction that may account for this can be expressed as follows:[50]

$$Mn(C_8H_4O_4)(H_2O)_2 + C^+ + e^- \leftrightarrow MnC(C_8H_4O_4)(H_2O)_2$$
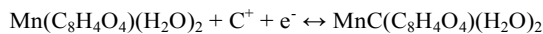
The CV curves under different scanning rates, from 5 to 100 mV s$^{-1}$, presented nearly rectangular feature, indicating a close-to-ideal pseudo-capacitive nature of the electrode. The CNTs@Mn-MOF composite exhibited a high specific capacitance of 206 F g$^{-1}$ at a scan rate of 5 mV s$^{-1}$, which decreased to 112.5 F g$^{-1}$ at a high scan rate of 100 mV s$^{-1}$. Note that, the capacitive contributions from blank carbon fiber paper are negligible (Fig. S2†). The exact rate performances were further evaluated by galvanostatic charge–discharge (GCD) measurements, the charging and discharging curves of different current rates, including 1, 2, 3, 4, 10 and 20 A g$^{-1}$ (Fig. S3†). All these curves present a symmetric feature, suggesting ideal pseudo-capacitive nature of fast charge/discharge processes. Accordingly, in a wide potential window of 1.0 V, the specific capacitance can reach 203.1 F g$^{-1}$ at a current density of 1 A g$^{-1}$. For Mn$^{II}$-based materials, there are only a few reports on the application of supercapacitors. It is worth noting that the specific capacitance of 203.1 F g$^{-1}$ reported here is much higher than that of some previous reported composites of mesoporous carbon@MnO[49] (160 F g$^{-1}$ at 1 A g$^{-1}$) and graphene oxide@MnO[50] (51.5 F g$^{-1}$ at 0.5 A g$^{-1}$). To the best of our knowledge, the obtained single-electrode capacitances of CNTs@Mn-MOF are superior to the available reports on Mn$^{II}$-based supercapacitor electrodes and spur the low capacitance of
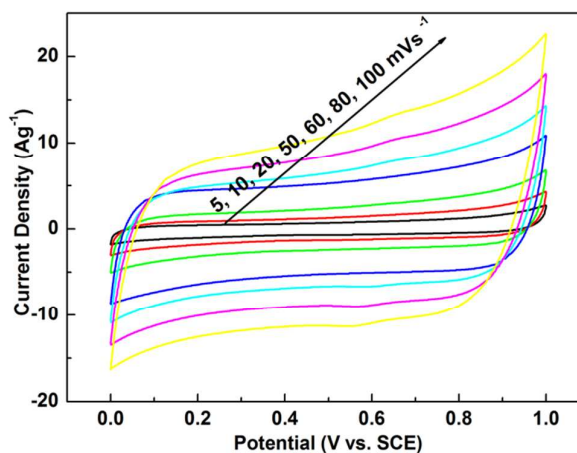


**Fig. 4** CV curves of CNTs@Mn-MOF tested by a three-electrode system at different scan rates in 1 M $Na_2SO_4$.

MnO materials to a higher level.

To confirm the influence of modification by CNTs on the supercapacitive properties of Mn-MOF material, we carried out electrochemical measurements in a three-electrode system with the three materials (Fig. 5). Both CV (all at 100 mV s$^{-1}$, Fig. 5a) and GCD (all at 1 A g$^{-1}$, Fig. 5c) tests of Mn-MOF and CNTs showed much lower capacitances when compared with that of CNTs@Mn-MOF. The maximum specific capacitances of CNTs@Mn-MOF, Mn-MOF and CNTs were 203.1, 43.2, 72.9 F g$^{-1}$ at a scan rate of 5 mV s$^{-1}$ and 202.8, 28.4, 60 F g$^{-1}$ at a current density of 1 A g$^{-1}$, respectively. A standard rectangular CV curve for CNTs with a potential window of 0.5 V (*vs.* SCE) indicated a feature of electrical double layer capacitors. The low capacitance of 72.9 F g$^{-1}$ (at 5 mV s$^{-1}$) was in the reported rang of 50-100 F g$^{-1}$ for CNTs, which was restricted by the single property of double layer capacity without faradic reactions.[52] CV curve of Mn-MOF was similar to that of CNTs@Mn-MOF, but with a relatively small area corresponded to a low capacitance, which was attributed to the poor conductivity of MOFs material. As clearly seen in Fig. 5b and Fig. 5d, the capacitance values of CNTs@Mn-MOF were 4.7-, 4.6-, 4.3-, 4.5-, 4.6-fold and 7.1-, 6.8-, 6.7, 11-, 15-fold higher than those of the composites at 5, 10, 20, 50, 100 mV s$^{-1}$ and 1, 2, 3, 10, 20 A g$^{-1}$ as well as pure Mn-MOF, respectively. As the results, it can be concluded here that adding CNTs to the Mn-MOF can overcome the poor electron conductive property of the MOFs material, which can lead to a much higher capacitance. This was also confirmed by Nyquist plots (Fig. S4†). The curves in low frequency were similar to each other while the slopes were steeper than 45° which associated with Warburg diffusion. The CNTs@Mn-MOF displayed a smaller semicircle at high frequencies than pure Mn-MOF, which illustrated that the kinetics performance of the material was improved by incorporation of CNTs. The *Rs* of CNTs@Mn-MOF, which was valued by the intercept of the real part of impedance with the x-axis, exhibited a significant decrease in
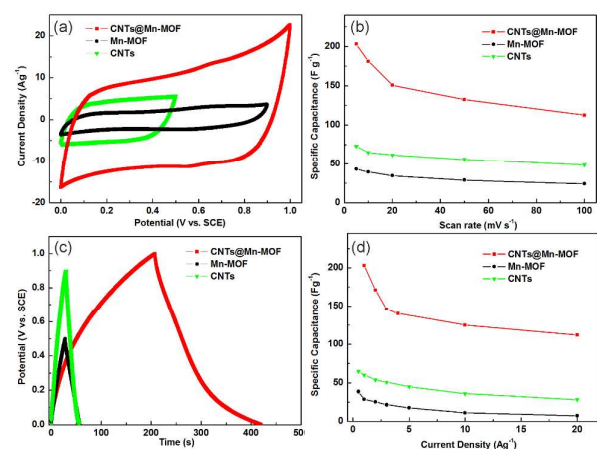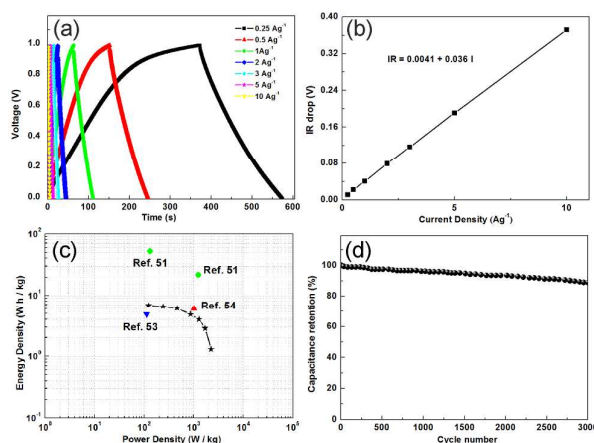


**Fig. 6** (a) GCD curves of symmetrical cells relative to current densities, (b) dependence of IR drop on current densities, (c) Ragone plot of the symmetrical cells, (d) cycle performance of symmetrical supercapacitor at 5 A g$^{-1}$.

comparison with pure Mn-MOF. Unsurprisingly, a slight increase of *Rs* was observed after long-term cycling, which was a normal behavior due to changes of material structure. This results indicated that the resistance of the electrolyte, intrinsic resistance of the substrate and contact resistance of MOF material were effectively improved by the incorporation of CNTs. As inside of the hybrid material, the CNTs were tightly attached to the MOF inwall, which was beneficial for mechanical reinforcement and enhancing electronic conduction. The important role of the CNTs in the structure on charge storage was due to their effects on regulating the electrical contact pathways between adjacent particles and providing an electron transport network. Therefore, the characteristics combination of Mn-MOF and CNTs leads to not only a dramatic improvement in electrical conductivity but also in specific capacitance.

In order to demonstrate the practical performance of CNTs@Mn-MOF, a symmetrical supercapacitor device was fabricated using the hybrid material as electrodes and one piece of polypropylene membrane as a separator. As presented by typical GCD curves under various current densities in Fig. 6a, the optimized symmetrical cell can provide a maximum specific capacitance of 50.3 F g$^{-1}$ at 0.25 A g$^{-1}$. When the current densities increases to 0.5, 1, 2, 3, 5 and 10 A g$^{-1}$, the specific capacitance of the symmetrical cell decreases to 48.9, 47.7, 40.8, 36.9, 31.2 and 23.4 F g$^{-1}$, retaining 97.4%, 95%, 81.6%, 73.8%, 62% and 59.6% of its value at 0.25 A g$^{-1}$, respectively. The excellent rate performances were due to the Mn-MOF incorporated with functionally CNTs. It is accepted that the capacitance gradually decreases with the increase of current density, which is attributed to the low utilization of active materials under high charge-discharge current densities. Fig. 6b shows the dependence of *IR* drop on applied current density, and it was fitted to a linear plot. The slop demonstrates corresponding internal resistance. As for the well-fitted line (*IR* = 0.0041 + 0.036 *I*), the initial voltage loss was small even at



**Fig. 5** (a) CV curves in 1M Na$_2$SO$_4$ at 100 mV s$^{-1}$, (b) the specific capacitances vs. scan rates, (c) GCD curves at 1 A g$^{-1}$, and (d) the specific capacitances vs. applied current densities.

high current densities, indicating a low internal resistance and fast *I-V* response in the symmetrical supercapacitor.

Fig. 6c displays typical Ragone plots (power density vs. energy density), with an operation voltage of 1 V. This symmetrical device exhibited an energy density of 6.9 Wh kg$^{-1}$ at a power density of 122.6 W kg$^{-1}$. In addition, the power density can reach 2240 W kg$^{-1}$ when maintaining the energy density of 1.3 Wh kg$^{-1}$. Up to now, Mn-MOF supercapacitor has not been reported. Therefore, we selected a composite of MnO@NCS,[51] a symmetrical supercapacitor of MnO$_2$[53] and a nanocomposite of CNT/MnO$_2$[54] to make a comparison with our work. Obviously, the symmetrical supercapacitor in our work displays much better performance. Fig. 6d shows the long-term cycling stability of the symmetrical supercapacitor, measured by the GCD technique at 5 A g$^{-1}$.The capacitance retentions for the symmetrical supercapacitor was still maintained at 88% of its highest value after 3000 cycles (SEM image in Fig. S5†), indicating that the CNTs@Mn-MOF material not only had an excellent specific capacitance but also had an outstanding cycling stability. This cycling stability is superior to the typical MnO$_x$-based supercapacitor.[55,56]

## Conclusions

In summary, a composite of CNTs@Mn-MOF was synthesized via a facile hydrothermal process. In the constructive structure, the CNTs act as strongly mechanical supports and conductive networks for the hybrid MOF material. An excellent capacitance of 203.1 F g$^{-1}$ was achieved in a three electrode system. In addition, the symmetrical supercapacitor showed good performance within the maximum energy density of 6.9 Wh kg$^{-1}$ and maximum power density of 2240 W kg$^{-1}$. Moreover, 88% of its highest specific capacitance was maintained after 3000 cycles at 5 A g$^{-1}$. The present study indicates the CNTs@Mn-MOF as a potential candidate for Mn-based supercapacitors and brings new method to improve supercapacitive performance of various MOFs material. We believe that this hybrid MOFs composite can open the door to develop new materials in electrical energy storage.

## Acknowledgements

## Notes and references

1 J. Wang, H. Tang, H. Ren, R. Yu, J. Qi, D. Mao, H. Zhao and D. Wang, *Adv. Sci.*, 2014, **1**, 1400011.

2 W. F. Wei, X. W. Cui, W. X. Chen, D. G. Ivey, *Chem. Soc. Rev.*, 2011, **40**, 1697.

3 R. Liu and S. B. Lee, *J. Am. Chem. Soc.*, 2008, **130**, 2942.

4 S. W. Zhang and G. Z. Chen, *Energy Mater.*, 2008, **3**, 186.

5 F. Y. Yang, M. S. Zhao, Q. J. Sun, *RSC Adv.*, 2015, **5**, 9843.

6 S. L. Chen, F. Liu, Q. J. Xiang, *Electrochim. Acta*, 2013, **106**, 360.

7 G. Yu , L. Hu, M. Vosgueritchian, H. Wang, X. Xie, J. R. McDonough, X. Cui, Y. Cui, Z. Bao, *Nano Lett.*, 2011, **11**, 2905.

8 C. Liu, F. Li, L. P. Ma, H. M. Cheng, *Adv. Mater.*, 2010, **22**, E28.

9 T. Brousse, M. Toupin, R. Dugas, L. Athouel, O. Crosnier and D. Belanger, *J. Electrochem. Soc.*, 2006, **153**, A2171.

10 O. Ghodbane, J. L. Pascal and F. Favier, *ACS Appl. Mater. Interfaces*, 2009, **1**, 1130.

11 R. N. Reddy and R. G. Reddy, *J. Power Sources*, 2003, **124**, 330.

12 X. Jin, W. Zhou, S. Zhang and G. Z. Chen, *Small*, 2007, **3**, 1513.

13 S. B. Ma, K. Y. Ahn, E. S. Lee, K. H. Oh and K. B. Kim, *Carbon*, 2007, **45**, 375.

14 Z. Yu, B. Duong, D. Abbitt and J. Thomas, *Adv. Mater.*, 2013, **25**, 3302.

15 M. Nakayama, A. Tanaka, S. Konishi and K. Ogura, *J. Mater. Res.*, 2004, **19**, 1509.

16 H. Xia, C. Hong, X. Shi, B. Li, G. Yuan, Q. Yao and J. Xie, *J. Mater. Chem. A*, 2015, **3**, 1216.

17 E. C. Rios, A. V. Rosario, R. M. Q. Mello and L. Micaroni, *J.Power Sources*, 2007, **163**, 1137.

18 S. R. Sivakkumar, J. M. Ko, D. Y. Kim, B. C. Kim and G. G. Wallace, *Electrochim. Acta*, 2007, **52**, 7377.

19 S. L. James, *Chem. Soc. Rev.*, 2003, **32**, 276.

20 A. Corma, H. Garcia and F. X. Llabresi Xamena, *Chem. Rev.*, 2010, **110**, 4606.

21 A. U. Czaja, N. Trukhan and U. Mueller, *Chem. Soc. Rev.*, 2009, **38**, 284.

22 P. Horcajada, T. Chalati, C. Serre, B. Gillet, C. Sebrie, T. Baati, J. F. Eubank, D. Heurtaux, P. Clayette, C. Kreuz, J. S. Chang, Y. K. Hwang, V. Marsaud, P. N. Bories, L. Cynober, S. Gil, G. Ferey, P. Couvreur and R. Gref, *Nat. Mater.*, 2010, **9**, 172.

23 L. E. Kreno, K. Leong, O. K. Farha, M. Allendorf, R. P. Van Duyne and J. T. Hupp, *Chem. Rev.*, 2012, **112**, 1105.

24 H. Wu, W. Zhou and T. Yildirim, *J. Am. Chem. Soc.*, 2007, **129**, 5314.

25 N. L. Rosi, J. Eckert, M. Eddaoudi, D. T. Vodak, J. Kim, M. O. Keeffe and O. M. Yaghi, *Science*, 2003, **300**, 1127.

26 F. Vilela, K. Zhang and M. Antonietti, *Energy Environ. Sci.*, 2012, **5**, 7819.

27 C. Y. Su, A. M. Goforth, M. D. Smith, P. J. Pellechia and H. C. zurLoye, *J. Am. Chem. Soc.*, 2004, **126**, 3576.

28 F. Meng, Z. G. Fang, Z. X. Li, W. W. Xu, M. J. Wang, Y. P. Liu, J. Zhang, W. R. Wang, D. Y. Zhao and X. H. Guo, *J. Mater. Chem. A*, 2013, **1**, 7235.

29 H. L. Jiang, B. Liu, Y. Q. Lan, K. Kuratani, T. Akita, H. Shioyama, F. Zong and Q. Xu, *J. Am. Chem. Soc.*, 2011, **133**, 11854.

30 A. J. Amali, J. K. Sun and Q. Xu, *Chem. Commun.*, 2014, **50**, 1519.

31 D.Y. Lee, S.J. Yoon, N.K. Shrestha, S.-H. Lee, H. Ahn, S.-H. Han, *Microporous Mesoporous Mater.*, 2012, **153**, 163.

32 D. Y. Lee, D. V. Shinde, E. K. Kim, W. Lee, I. W. Oh, N. K. Shrestha, J. K. Lee and S. H. Han, *Microporous Mesoporous Mater.*, 2013, **171**, 53.

33 Y. Gong, J. Li, P. G. Jiang, Q. F. Li and J. H. Lin, *Dalton Trans.*, 2013, **42**, 1603.

34 M. Du, M. Chen, X. G. Yang, J. Wen, X. Wang, S. M. Fang and C. S. Liu, *J. Mater. Chem. A*, 2014, **2**, 9828.

35 N. Campagnol, R. Romero-Vara, W. Deleu, L. Stappers, K. Binnemans, D. E. De Vos and J. Fransaer, *ChemElectroChem*, 2014, **1**, 1182.

36 Jie Yang, Peixun Xiong, Cheng Zheng, Heyuan Qiu and Mingdeng Wei, *J. Mater. Chem. A*, 2014, **2**, 16640

37 Jie Yang, Cheng Zheng, Peixun Xiong, Yafeng Li and Mingdeng Wei, *J. Mater. Chem. A*, 2014, **2**, 19005.

38 K. M. Choi, H. M. Jeong, J. H. Park, Y. B. Zhang, J. K. Kang and O. M. Yaghi, *ACS Nano*, 2014, **8**, 7451.

39 P. Srimuk, S. Luanwuthi, A. Krittayavathananon and M. Sawangphruk, *Electrochim. Acta*, 2015, **157**, 69.

40 J. T. Han, S. Y. Kim, J. S. Woo, G.-W. Lee, *Adv. Mater.*, 2008, **20**, 3724.

41 S. Berson, R. De Bettignies, S. Bailly, S. Guillerez, B. Jousselme, *Adv. Funct. Mater.*, 2007, **17**, 3363.

42 S. J. Yang, J. Y. Choi, H. K. Chae, J. H. Cho, K. S. Nahm and C. R. Park, *Chem. Mater.*, 2009, **21**, 1893.

43 Z. H. Xiang, Z. Hu, D. P. Cao, W. T. Yang, J. M. Lu, B. Y. Han and W. C. Wang, *Angew. Chem., Int. Ed.*, 2011, **50**, 491.

44. M. Shoaee, M. W. Anderson and M. P. Attfield, *Angew. Chem., Int. Ed.*, 2008, **47**, 8525.

45 J. A. Kaduk, *Acta Crystallogr., Sect. B*, 2002, **58**, 815.

46 M. A. Stranick, *Surface Science Spectra*, 1999, **6**, 47.

47 F. Zhang, L. Hao, L. J. Zhang and X. G. Zhang, *Int. J. Electrochem. Sci.*, 2011, **6**, 2943.

48 Q. Y. Liao, N. Li, H. Cui and C. X. Wang, *J. Mater. Chem. A*, 2013, **1**, 13715.

49 T. Wang, Z. Peng, Y. Wang, J. Tang and G. Zheng, *Sci. Rep.*, 2013, **3**, 2693.

50 D. Antiohos, K. Pingmuang, M. S. Romano, S. Beirne, T. Romeo, P. Aitchison, A. Minett, G. Wallace, S. Phanichphant and J. Chen, *Electrochim. Acta*, 2013, **101**, 99-108.

51 M. Yang, Y. Zhong, X. Zhou, J. Ren, L. Su, J. Wei and Z. Zhou, *J. Mater. Chem. A*, 2014, **2**, 12519.

52 L. L. Zhang, R. Zhou and X. S. Zhao, *J. Mater. Chem.*, 2010, **20**, 5983.

53 S. Nagamuthu, S. Vijayakumar and G. Muralidharan, *Ind. Eng. Chem. Res.*, 2013, **52**, 18262.

54 Y. Jin, H. Chen, M. Chen, N. Liu, Q. Li, *ACS Appl. Mater. Interfaces*, 2013, **5**, 3408.

55 X. Zhao, L. Zhang, S. Murali, M. D. Stoller, Q. Zhang, Y. Zhu and R. S. Ruoff, *ACS Nano*, 2012, **6**, 5404.

56 L. Mao, K. Zhang, H. S. O. Chan and J. S. Wu, *J. Mater. Chem.*, 2012, **22**, 1845.